PCCP

Theoretical determination of a model molecule for the catalytic upcycling of polyethylene and polypropylene

Journal:	*Physical Chemistry Chemical Physics*
Manuscript ID	CP-ART-12-2024-004663.R1
Article Type:	Paper
Date Submitted by the Author:	05-May-2025
Complete List of Authors:	Ortega-Ramos, Jessica; Texas Tech University Maraschin, Mikael; Texas Tech University Botte, Gerardine; Texas Tech University Gauthier, Joseph; Texas Tech University

ARTICLE

Theoretical determination of a model molecule for the catalytic upcycling of polyethylene and polypropylene

Received 00th January 20xx,
Accepted 00th January 20xx

DOI: 10.1039/x0xx00000x

Jessica Ortega-Ramos,[a,b] Mikael Maraschin,[b] Gerardine G. Botte*[a,b] and Joseph A. Gauthier*[b]

Considering the severe environmental and humanitarian implications of global plastic waste accumulation, understanding polyolefin catalytic breakdown is essential. Accordingly, a model compound would improve the reproducibility of experiments and simplify theoretical models. Therefore, this study aimed to determine the minimum number of monomers necessary to represent the breakdown of polyethylene and polypropylene over metal catalysts. Using density functional theory (DFT) calculations, we evaluated how the polymer's chain length affects reaction energies and energy barriers for C-H and C-C cleavage over stepped transition metal surfaces. We found that chain length does not significantly affect the C-H and C-C cleavage reaction energies and the C-H cleavage energy barriers. Our findings suggest that a small oligomer (less than 10 carbons) could be suitable as a model to study polyethylene's catalytic C-H and C-C cleavage. Although such a simple molecule cannot capture complex transport, entanglement phenomena, and product selectivity observed in full polymers, it may prove useful for determining reaction energetics in complex systems and accelerating catalyst screening.

1 Introduction

Plastic waste rapidly accumulates in terrestrial and aquatic landscapes, severely threatening human health and the environment. In 2019, only 9% of plastics were recycled globally, while 49% ended up in landfills, 19% were incinerated, and 22% were disposed of into uncontrolled dumpsites (possibly leading to accumulation in bodies of water) or burned in open pits.[1,2] Significant components of this plastic waste are polyethylene (PE) and polypropylene (PP), both of which are produced on an enormous scale and are utilized specifically for their exceptional stability over extended timescales.[3] Traditional methods for polyolefin upcycling,[4] like pyrolysis,[5] hydrogenolysis,[6] and solvolysis,[7] are energy-intensive or require toxic/flammable chemicals, and suffer from known selectivity challenges. Alternatively, new approaches like biodegradation,[8] photocatalysis,[9] and electrocatalysis[10] are performed in relatively mild conditions but typically suffer from low conversion efficiencies, slow kinetics,[11] and as-of-yet unresolved mass transport challenges.

To effectively improve upon new and existing upcycling methods, gaining a molecular-level understanding of the catalytic C-C and C-H bond scission through highly reproducible experimental and theoretical studies is essential. Yet, fundamental research of this kind is challenging due to the size and complexity of the polymer structure, which involves different degrees of crystallinity, branching, molecular weight, and the presence of impurities and additives that can significantly modify its reactivity.[12] A model molecule with similar chemical reactivity would simplify the theoretical analysis and significantly improve the reproducibility of experiments, given the higher availability of pure, well-characterized, low molecular weight compounds. However, to our knowledge, no general criteria exist in the literature to select a compound that accurately represents the same chemistry as the polymer for the heterogeneous catalytic activation of the C-H and C-C bonds. In published literature reports studying polyethylene, when simplification was needed, the selection of the chain length was made to fit the necessities of the particular experiment, but without clear universal criteria.[13–16]

The number of monomers needed to observe convergence in the kinetics and thermodynamics of C-C bond cleavage in the gas phase was investigated previously. Knyazev[17] demonstrated through molecular dynamic simulations that the per-bond rate constant for thermal C-C bond breaking increases with the chain length from ethane (C2) to decane (C10), but between C10 and C50, there was no significant change in the per-bond rate constant. Also, Alkorta and Elguero[18] calculated the bond dissociation energies (BDE) of C-C bonds in n-alkanes of increasing chain length from ethane to decane at different theory levels: G2MP2, G2, G3MP2B3, G3, and G3B3 within the Gaussian-03 package. The authors observed that the BDE of the middle C-C bond stabilizes after ten carbons to a value of -371.8 kJ mol^{-1}, corresponding to the n-alkane of infinite length. Both reports importantly focused on the gas-phase cleavage of the C-C bond in an isolated molecule. However, critically, the effect of chain length on C-C bond-scission over a catalyst has, to our knowledge, not been explored. It is essential to evaluate this type of system since heterogeneous catalysis can break down polyolefins at substantially milder conditions and with higher selectivity than the uncatalyzed gas-phase process.

Previous studies[17,18] determined that ten carbons are sufficient to represent the C-C bond cleavage of polyethylene, enabling

[a] Institute for Sustainability and Circular Economy, Department of Chemical Engineering, Texas Tech University. E-mail: Gerri.Botte@ttu.edu
[b] . Department of Chemical Engineering, Texas Tech University, Texas Tech University. E-mail: Joe.Gauthier@ttu.edu

Supplementary Information available: Machine learning fine tuning details and supporting figures (PDF). Optimized structures and necessary data to reproduce the figures (ZIP). See DOI: 10.1039/x0xx00000x

precise determination of thermodynamic properties through quantum-chemical analysis in the gas phase. However, this statement is not applicable to molecules bound to a surface. On the surface, the number of possible conformations and binding sites that need to be sampled to find the global minimum of the system increases combinatorically as the chain length increases. Moreover, the unit cell size required to fit the oligomer also increases for longer hydrocarbons (adding more atoms to the calculation), especially if a low surface coverage is desired. Therefore, it is critical to investigate if a link between a more tractable molecule and polyethylene can be established in the context of heterogeneous catalysis.

This study aimed to determine the minimum chain length required to accurately represent the degradation and functionalization of polyethylene and polypropylene over a metal catalyst. To achieve this, density functional theory (DFT) calculations were conducted to evaluate the impact of chain length on the reaction energies and energy barriers associated with the C-H and C-C bond cleavage of polyethylene and polypropylene oligomers on Pt(211) and other transition metals. These results represent the first step in defining a polyethylene and polypropylene model molecule in heterogeneous systems, which will bring the opportunity to conduct more reproducible experiments and carry out theoretical studies in catalyzed polyolefin upcycling and recycling.

2 Computational details

Periodic, plane wave density functional theory (DFT) calculations were performed using Vienna ab initio simulation package (VASP),[19,20] interfaced through the Atomic Simulation Environment (ASE).[21] Core electrons of each atom were described with projector augmented wave (PAW) pseudopotentials,[22] and valence electrons were modeled by plane waves up to a kinetic energy cutoff of 500 eV. The revised Perdew-Burke-Ernzerhof (RPBE) functional form of the generalized gradient approximation (GGA)[23] was used to address the exchange-correlation effects, and Grimme's DFT-D3 method[24] with the zero-damping function was used to describe the van der Waals interactions semiempirically. The convergence criterion for the geometry optimizations was when the residual forces were smaller than 0.03 eV $Å^{-1}$. The convergence criterion for the electronic energy in each electronic self-consistency cycle was when the difference between iterations was not more than 10^{-4} eV. The electronic occupancies were determined according to the Gaussian smearing method with a smearing width of 0.05 eV.

Calculations of gas phase species were performed in a 20 x 20 x 40 Å unit cell of vacuum and were computed using a 2 x 2 x 1 Monkhorst-Pack k-point grid. The (211) surface of the fcc metal was selected to carry out the C-H and C-C cleavage due to the higher reactivity of its undercoordinated atoms located at the step.[25] The selection of the surface was made only to facilitate the cleavage of the C-C and C-H bonds, and studying how these bonds break on different surfaces is beyond the scope of this work. The lattice constant for platinum was optimized without the vdW correction enabled because it tends to substantially reduce the lattice constant. As a result, our surface calculations where the vdW correction is enabled are likely to be 1% strained. Still, this strain did not affect the linear trends observed for the reaction energies (see Figure S1 of the Supplementary Information).

For the calculations involving species bound to the metal surface, the supercell size depended on the type of bond being broken (C-H or C-C bond cleavage). For the C-H bond cleavage, a 12x3x3 supercell was used to accommodate the larger hydrocarbon chains along the x-direction. For the C-C bond cleavage, 9x3x3 (polyethylene) and 9x8x3 (polypropylene) supercells were used to fit the segments produced after breaking the C-C bond. All the supercells had three layers of atoms where the first layer was allowed to relax, and the other two layers were constrained to the bulk positions. A vacuum region of 10 Å separated the successive slabs to avoid periodic interactions, and a dipole correction was included.[26] In these calculations, the Brillouin zone was sampled with a 32/a x 40/b x 1 Monkhorst-Pack k-point grid, where a and b are the lattice vectors parallel to the XY-plane of the cell. Finally, it was confirmed that the energy values and trends found were independent of the supercell size (see Figure S2 of the Supplementary Information)

The transition states were first estimated by constraining the distance between the cleaved hydrogen and the oligomer and calculating the energy at different constrained distances. The highest energy structure was considered the approximate transition state. Then, more accurate transition state structures were obtained using the dimer method as developed and implemented by Henkelman.[27] A force tolerance of 0.01 eV $Å^{-1}$ is used in all the transition state searches. We confirmed the localization of a true saddle point by finite difference estimation of the Hessian and identification of a single imaginary vibrational frequency, except where noted otherwise.

The minima hopping global optimization method,[28] implemented through ASE with a temperature of 300 K, was used to find the minimum energy configuration for the structure consisting of the metal slab with the hydrocarbon after the C-H or C-C cleavage. A Hookean constraint with a cutoff distance of 1.59 Å and k = 7 was placed between the C-H and C-C bonds of the n-alkane to prevent undesired spontaneous cleavage of these bonds aside from the bond of interest. The calculator used for this method was the Open Catalyst Project[29] calculator, which is based on a machine-learning model to determine the energies and forces of the atomic structure. The machine learning model was fine-tuned to the hydrocarbon and metal surface system using the procedure described in the Supplementary Information.

3 Results

Before analyzing the trends in the reaction energies and energy barriers, we report the approaches taken in this work to determine them, in particular, the use of generalized machine learning potentials to find lower energy configurations of the

system, the handling of the supercell size effect in the calculations, and the selection of the proper initial state.

3.1 Machine learning potentials

A fine-tuned machine learning model was used as a substitute for the DFT relaxation step needed in the minima hopping,[28] accelerating the process of screening hundreds of configurations to search for the one with the lowest energy. The machine learning model was developed by the Open Catalyst Project (OCP), a collaborative research effort between Fundamental AI Research (FAIR) at Meta AI and Carnegie Mellon University's (CMU) Department of Chemical Engineering.[30] The model consists of a Graph Neural Network (GNN), where each graph is represented by a set of vertices (atoms) and edges (interactions between atoms).[29] One of the main tasks of the model is to predict the energy and forces given a structure as input. Although the dataset for this model includes more than 200 million structures involving metal (OC20)[31] and oxide (OC22)[32] slabs with and without a variety of adsorbates, these small adsorbates (five atoms on average) are considerably different from the long hydrocarbons studied in this work. This difference caused poor accuracy in the off-the-shelf prediction of the system's total energy for a dataset created from DFT relaxations of PE and PP oligomers over Pt(211), illustrated by the parity plot of Figure 1 (a) and the relatively large mean absolute error (MAE) of 0.452 eV/atom.

As a result, the machine learning model required fine-tuning.[33] For this procedure, a training set was created using several DFT geometry optimizations for the final state of C-H and C-C bond cleavage of PE and PP oligomers over Pt(211), gathering a total of over 1600 trajectories. To prevent overfitting, we limited fine-tuning to 10 epochs and implemented an early stopping method with a maximum number of 3 epochs without improvement. This approach prevents the model from entering the interpolation region where validation loss increases with the number of epochs (Figure S3, Supplementary Information). The absence of overfitting was confirmed by the generalization error, provided from the test set, which would have shown a higher MAE (0.0016 eV/atom) than the training set (0.0015 eV/atom) if overfitting had occurred. After the fine-tuning, the model's performance improved significantly, as demonstrated by the parity plot in Figure 1 (b).

The fine-tuned machine learning model was used in the relaxation and annealing steps of the minima hopping. This approach made it possible to quickly find a lower energy configuration compared to the starting configuration in most cases. For instance, the energy distribution, relative to the minimum energy, for the 300 configurations found for the system of a Pt(211) slab with an adsorbed octane is shown in Figure 1 (c). In this figure, most configurations differ from the minimum energy configuration by 0.3 eV. The difference between the geometry of the lowest and highest energy configurations is illustrated in Figure 1(d), where the starting configuration is also shown for comparison. Here, the main difference between the configurations is the orientation of the octane over the surface, which can cause an energy difference as high as 0.7 eV. It is important to note that minima hopping employed with the fine-tuned machine learning model did not always find a lower energy configuration, and when it did, this configuration is not necessarily guaranteed to be the global minimum of the system.

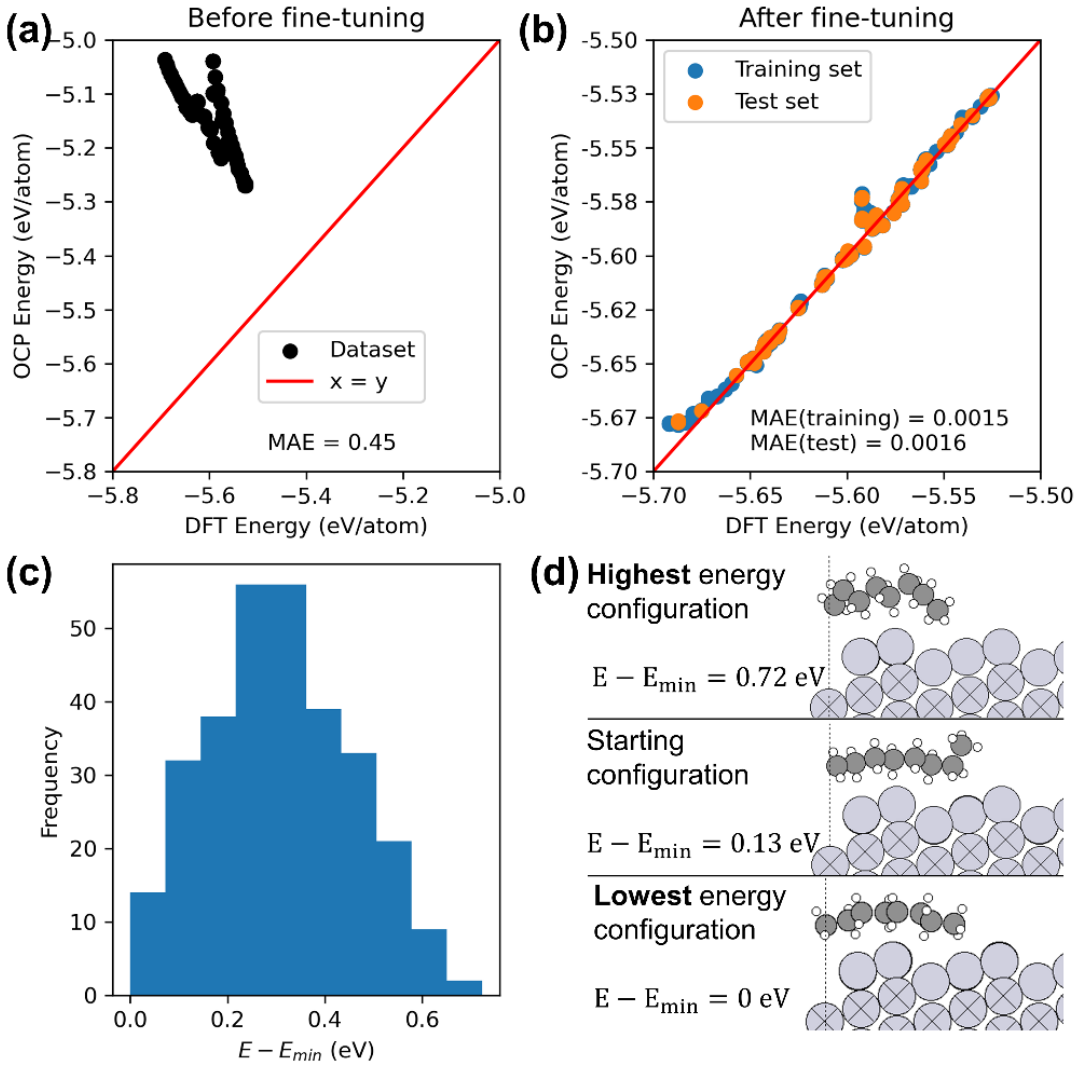

Figure 1. (a) Parity plot showing the correspondence between the DFT energy and the prediction made by the machine learning model using the GemNet-OC OC20+OC22 checkpoint (OCP energy) for the dataset of 2005 images created in this work. The mean absolute error (MAE) is in units of eV/atom. (b) Parity plot showing the correspondence between the DFT and OCP energy (after the fine-tuning) for the training and test datasets. (c) Distribution of the configuration's energies, relative to the lowest energy configuration (Emin), for the system consisting of octane adsorbed over a platinum slab. (d) Starting configuration, the highest and lowest energy configurations of the system (platinum slab + adsorbed octane) found using minima hopping.

3.2 Selection of initial state

Aside from finding the minimum energy configuration, another important consideration was the selection of the initial state when the final state is the cleaved bond (C-H or C-C) in the middle carbon over the metal surface, for which there are two possibilities to consider. In the first case, the initial state combines the gas-phase hydrocarbon and the clean platinum slab. For simplicity, we denote the reaction energies calculated with this initial state as RE1. Although this initial state is well-defined, the RE1s highly depend on the van der Waals attractive interactions between the hydrocarbon and the metal. This dependency is evidenced by the linear decrease in the RE1 as the number of monomers increases, as shown in Figure 2 (a), which follows the same trend as the adsorption energies for n-alkanes over a metal surface reported in the literature[34–36] and calculated in this work. We attribute the linear trend to the direct proportionality of the vdW interaction and the surface area of the hydrocarbon; no linear trend is observed when the vdW correction is omitted from the calculation (c.f. Figure S4 in the Supplementary Information). The linear behavior of the RE1s is not specific to platinum since it also occurs in other metals, as shown in Figure 2 (b). In all these cases, the RE1s follow the same linear trend as the adsorption energies with a similar slope within a 10% error (c.f. Figures S5 to S8 in the Supplementary Information).

In the second case, which we denote as RE2, the initial state is the physically adsorbed hydrocarbon over the platinum surface. This initial state would allow subtraction of the hydrocarbon-metal interaction to see the effect of increasing the number of monomers in the C-H and C-C bond strength. However, the adsorbed hydrocarbon is more difficult to unambiguously define since there are many ways in which the hydrocarbon can

adsorb to the metal surface, and the number of possible configurations grows combinatorically as hydrocarbon chain length increases. Thus, finding the most stable absorption configuration (i.e., the global energy minimum of the system) for long hydrocarbon chains becomes challenging, even using minima hopping. The many possibilities for the adsorbed hydrocarbon introduce high variance to the RE2s when they are calculated as the difference between the adsorbed hydrocarbon (initial state) and the cleaved bond over the metal (final state) for each chain length (see Figure 2 (c), labelled as "difference: data points"). This result differs from the trend Ding et al.[36] reported, where the RE2s for the C-H cleavage of n-alkanes over Pt(111) and Pt_{55} cluster increased slightly with the number of carbons, from one to six carbons. The discrepancy between these results might be due to the difference in the range of n-alkanes evaluated. Smaller n-alkanes have fewer possible configurations; thus, the associated energies present lower variance. Also, the slight increase in the previously reported RE2s could be considered a small fluctuation due to the differences in adsorption configuration between the n-alkanes.

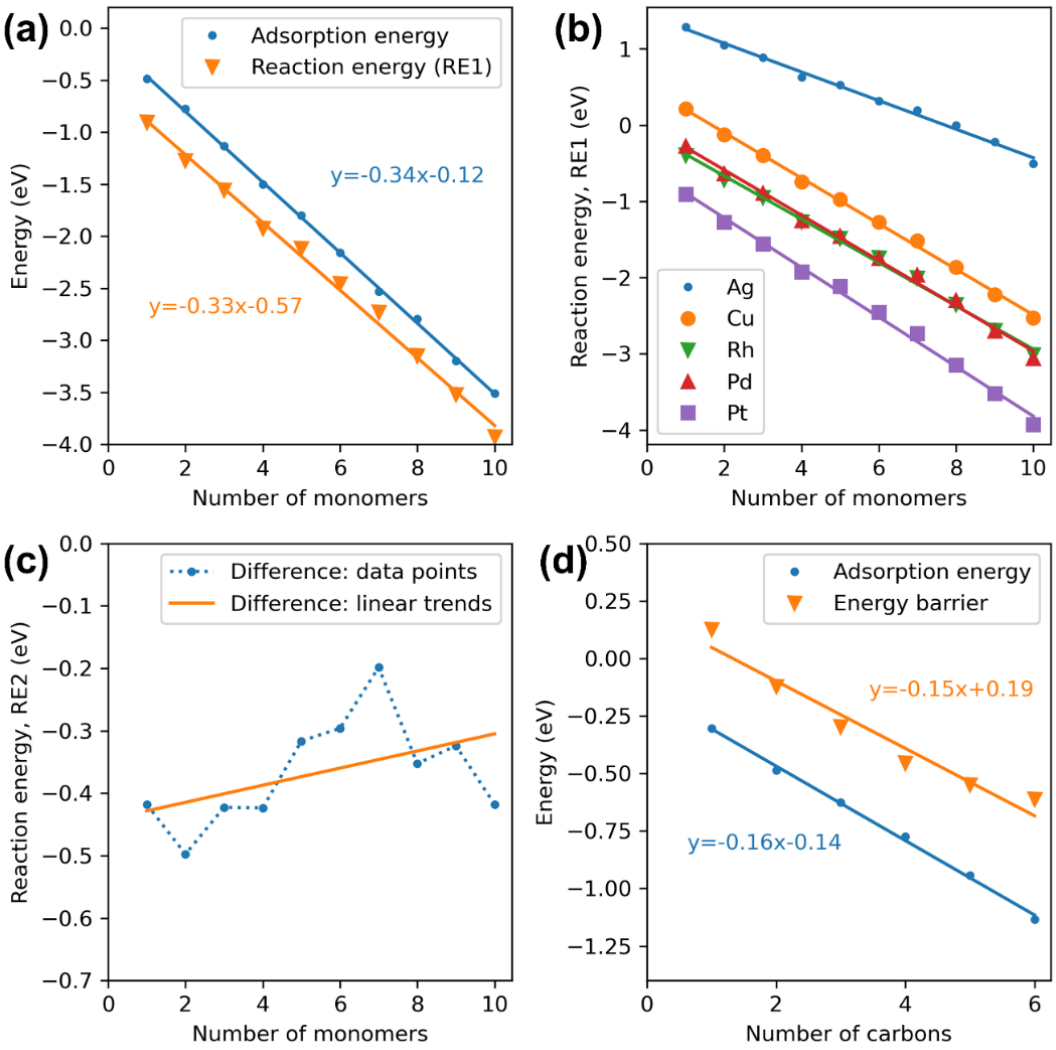

Figure 2. (a) Reaction energies for the C-H cleavage in the middle carbon (referred to as RE1 since the initial state is the clean metal slab and gas-phase hydrocarbon) and adsorption energies as a function of the number of monomers in the polyethylene oligomers over Pt(211). One monomer is equivalent to an ethane molecule. (b) RE1 for the C-H cleavage in the middle carbon as a function of the number of monomers in the polyethylene oligomers for different metals. (c) Reaction energies for the C-H cleavage in the middle carbon (RE2 since the initial state is the adsorbed hydrocarbon) as a function of the number of monomers in the polyethylene oligomers. The RE2s were calculated in two different ways: by the difference between the data points and by the difference between linear trends. (d) Energy barriers for the C-H cleavage in the middle carbon and adsorption energies as a function of the number of carbons in the n-alkane.

3.3 Reaction energies and energy barriers

An alternative approach to determining RE2 is to calculate the difference between the linear trends for the adsorption energy and RE1 found in Figure 2 (a). The result of this calculation, as shown in Figure 2 (c) (labeled as "difference: linear trend"), is that RE2 slightly increases as the number of monomers increases, but the overall change is essentially negligible. This result is evident from the fact that the slopes for the linear trends of adsorption energies and RE1s are within ~10%. Considering only the thermodynamics, this result implies that

the system will release approximately the same energy for the C-H cleavage in adsorbed ethane and adsorbed polyethylene when the reaction is catalyzed over a metal surface.

Reaction rates are ultimately determined by kinetics, which in the typical formalism will largely be determined by activation barriers. Towards this end, the energy barriers, with the gas-phase hydrocarbon and the clean platinum slab as the initial state, are shown in Figure 2 (d), along with the adsorption energies for n-alkanes from one to six carbons. A smaller range of n-alkanes was explored in this case for two reasons: (1) the result from the reaction energies suggested that convergence might be achieved at a low number of polyethylene monomers, and (2) it was not possible to guarantee the localization of a genuine transition state for longer chains due to the presence of more than one imaginary frequency in the frequency analysis, even at tight convergence criteria for the forces (0.01 eV $Å^{-1}$) and the energies ($1x10^{-8}$ eV). For butane, pentane, and hexane, two imaginary frequencies were observed; however, the second imaginary frequency was significantly smaller than the first one (716.0 cm^{-1} vs 135.9 cm^{-1}). Also, the first imaginary frequency corresponded to the apparent direction of the reaction coordinate, while the second corresponded to a rotation of the entire molecule (except for butane, where it was the opposite). Thus, the second imaginary frequency (the first one in the case of butane) was disregarded from the analysis. In Figure 2 (d), the energy barriers and the adsorption energies follow the same linear trend and are parallel, as in Figure 2 (a). Therefore, it is expected that the energy *barriers*, calculated by the difference between the linear trends of Figure 2 (d), do not change significantly from one to six carbons, shown graphically in Figure S9 of the Supplementary Information. This result implies that once the hydrocarbon is adsorbed to the surface, a methane molecule would exhibit the same activity for the C-H cleavage as a polyethylene chain.

The results presented up to this point have focused on the C-H cleavage in polyethylene oligomers; we find the same trends in the case of the C-C cleavage. Figure 3 (a) shows the RE1s for the C-C cleavage of polyethylene oligomers and the adsorption energies, where the RE1s and adsorption energies exhibit the same linear trend and slope.

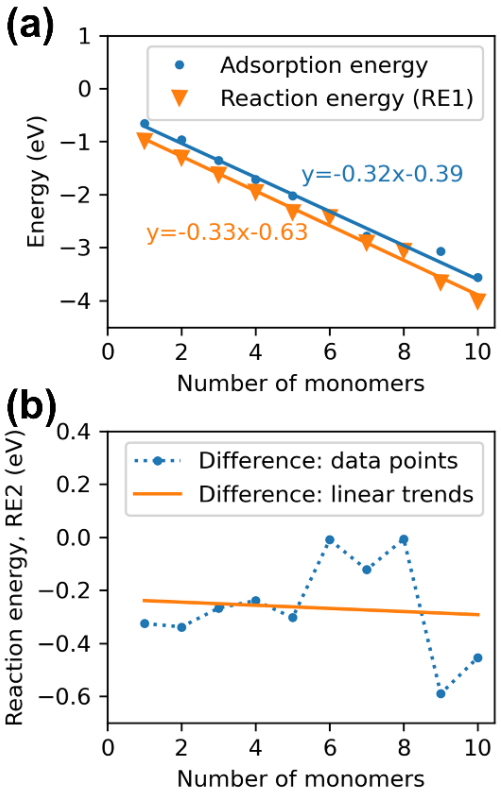

Figure 3. (a) Reaction energies for the C-C cleavage in the middle carbon (referred to as RE1 since the initial state is the clean metal slab and gas-phase hydrocarbon) and adsorption energies as a function of the number of monomers in the polyethylene oligomers. (b) Reaction energies for the C-C cleavage in the middle carbon (RE2 since the initial state is the adsorbed hydrocarbon) as a function of the number of monomers in the polyethylene oligomers. The RE2s were calculated in two different ways: by the difference between the data points and by the difference between linear trends.

The difference between these linear trends, which represent RE2, is shown in Figure 3 (b), along with the difference between data points. As we hypothesized, the RE2 calculated by the difference between linear trends presents no significant change as the number of monomers increased. Therefore, this result corroborates what was found for the C-H cleavage: an oligomer as small as ethane could represent the thermodynamics of the C-C cleavage of polyethylene over a metal surface.

For C-C bond cleavage, the energy barriers could not be determined since finding a transition state for the C-C cleavage of saturated n-alkanes over a metal surface was not possible: all transition state search routines we attempted through the NEB method converged to the C-C bond breaking in the gas phase before contacting the metal surface (see Figure S10 in the Supplementary Information). This event was considered unphysical, and the calculations where it happened were disregarded. Probably, the n-alkane must go through several dehydrogenation steps on the surface before the C-C bond can be broken, and this is supported by the exceptional stability of polyethylene. Still, we expect that the energy barriers will follow the same trend as the adsorption energies, as in the C-H cleavage case.

Finally, the results for the RE1s of C-H and C-C cleavage of PP oligomers are presented in Figure 4. In Figure 4 (a), the RE1s for

C-H cleavage and adsorption energies follow the same linear trend and are parallel. These features indicate that the RE2s do not change significantly with the number of monomers (see Figure S11 in the Supplementary Information). However, in Figure 4 (b), RE1s for the C-C cleavage follow a linear trend whose slope is slightly different from the slope for the linear trend of the adsorption energies. Qualitatively, this result suggests that the RE2s decrease indefinitely as the number of monomers increases, i.e., the RE2s tend to minus infinity as they approach the size of the full polymer. Most likely, the configurations found for the final state of the C-C cleavage and the adsorbed hydrocarbon are not the lowest energy configurations, despite extensive searching via minima hopping. This failure in finding the lowest energy configuration (or a configuration close to it) might be related to the bigger size and more complex structure of polypropylene oligomers compared to polyethylene oligomers, which increases the number of possible configurations over Pt(211) combinatorically and makes it harder to find the ones with the lowest energy. Since the linear trends might change considerably if lower energy configurations are found, and there is no agreement between the C-H and C-C bond cleavage trends, we find these results to be inconclusive, and a minimum chain length cannot be rigorously established from these results to represent the thermodynamics of C-H and C-C cleavage of PP over metal catalysts.

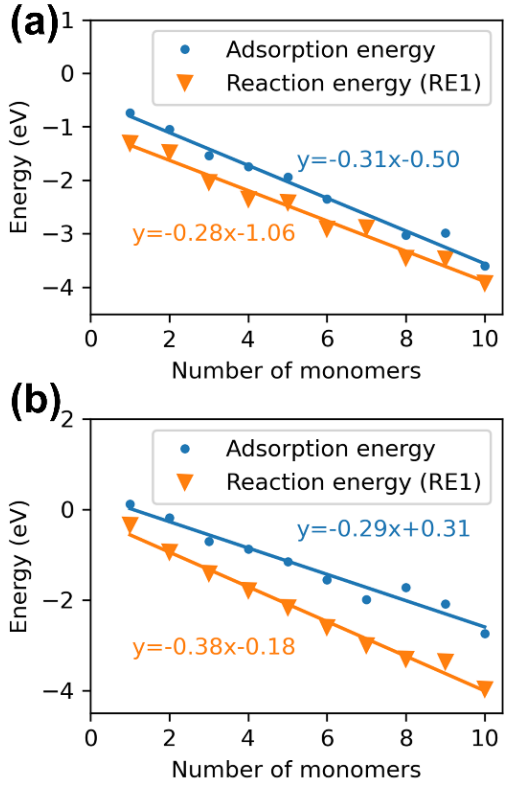

Figure 4. (a) Reaction energies for the C-H cleavage in the middle carbon (referred to as RE1 since the initial state is the clean metal slab and gas-phase hydrocarbon) and adsorption energies as a function of the number of monomers in the polypropylene oligomers. (b) RE1s for the C-C cleavage in the middle carbon and adsorption energies as a function of the number of monomers in the polypropylene oligomers.

4 Conclusions

We have performed DFT calculations to determine the effect of the number of monomers on the reaction energies and energy barriers of the C-H and C-C cleavage over a metal surface for polyethylene and polypropylene oligomers. Estimates of the global minimum energy configurations were found using minima hopping and a fine-tuned machine learning model. The fine-tuning of the machine learning model with data from this work decreased the initial MAE of 0.452 eV/atom to 0.0016 eV/atom for the test set, enhancing the accuracy of the energy prediction given an initial structure. The reaction energies of C-H and C-C bond cleavage were calculated using two different initial states: (1) the gas phase hydrocarbon and the clean metal slab (RE1) and (2) the adsorbed hydrocarbon over the metal slab (RE2). A linear relationship was observed between the RE1s and the number of monomers for polyethylene and polypropylene oligomers, which was attributed to the vdW interactions being proportional to the size of the molecule. The RE2s for the C-H and C-C cleavage and the energy barriers for the C-H cleavage were not affected by the size of the polyethylene oligomer.

Our findings suggest that an oligomer as small as ethane can be used as a model molecule for catalyst screening and computing the kinetics of polyethylene degradation, provided that the rate-determining step is the first C-H or C-C cleavage. If the rate-determining step is the formation of a C-O or C-X (X = halogen) bond, the energy trends might differ from those reported here. However, given the similar results for two different chemistries (C-H and C-C bond cleavage), we expect these energies to have the same trend of converging at very low number of carbons.

On the other hand, for polypropylene, it was not possible to conclusively determine the minimum length of the model molecule since there was a disagreement in the trends for the RE2s of the C-H and C-C bond cleavage.

The trends found in this work indicate the existence of simple rules to compute the energetics analogous to Benson group additivity,[37] which is prevalent in gas-phase reactions and has also been shown for intermediates on surfaces.[38] In this regard, the use of the fine-tuned machine learning model in conjunction with minima hopping can effectively compute the energetics of various oligomers on the metal surfaces, from which group additivity-like schemes can be built.

We again wish to highlight that using small molecules as a model for polyethylene, such as those studied here, will necessarily disregard important polymer behaviors such as entanglement and the significant mass transport challenges associated with catalytic polymer upcycling. Likewise, these molecules are unsuitable for studying product distribution or selectivity since they neglect the formation of chain fragments and cyclic/aromatic compounds. However, given the significant aforementioned challenges in conducting experiments with polymer systems – in addition to challenges in modeling polymer interactions at metal surfaces with DFT – our findings of simple molecules being suitable for reproducing critical polymer upcycling energetics will likely be useful in future studies.

Author contributions

Jessica Ortega-Ramos contributed to the formal analysis, investigation, visualization, and writing of the original draft. Mikael Maraschin contributed to the investigation, methodology, visualization, and writing of the original draft. Gerardine G. Botte contributed to funding acquisition, project administration, and review and editing of the draft. Joseph A. Gauthier was responsible for funding acquisition, conceptualization, methodology, formal analysis, project administration, supervision, and review and editing of the draft.

Conflicts of interest

There are no conflicts to declare.

Data availability

The data supporting this article have been included as part of the Supplementary Information.

Acknowledgments

This research was supported by the US Department of Energy, Office of Science, Office of Basic Energy Sciences, Chemical Upcycling of Polymers Program under Award DE-SC0022307. M.M. and J.A.G. acknowledge the Donors of the American Chemical Society Petroleum Research Fund for partial support of this research.

References

1 OECD, Plastic waste by end-of-life fate - projections, https://www.oecd-ilibrary.org/content/data/3f85b1c2-en.
2 C. Bremer, Plastic pollution is growing relentlessly as waste management and recycling fall short, says OECD, https://www.oecd.org/en/about/news/press-releases/2022/02/plastic-pollution-is-growing-relentlessly-as-waste-management-and-recycling-fall-short.html, (accessed August 19, 2024).
3 R. Geyer, J. R. Jambeck and K. L. Law, *Sci. Adv.*, 2017, **3**, e1700782.
4 J. Sun, J. Dong, L. Gao, Y.-Q. Zhao, H. Moon and S. L. Scott, *Chem. Rev.*, 2024, **124**, 9457–9579.
5 L. Zou, R. Xu, H. Wang, Z. Wang, Y. Sun and M. Li, *Natl. Sci. Rev.*, 2023, **10**, nwad207.
6 A. Musa, E. A. Jaseer, S. Barman and N. Garcia, *Energy Fuels*, 2024, **38**, 1676–1691.
7 W. Zhang, S. Kim, L. Wahl, R. Khare, L. Hale, J. Hu, D. M. Camaioni, O. Y. Gutiérrez, Y. Liu and J. A. Lercher, *Science*, 2023, **379**, 807–811.
8 S. Ghatge, Y. Yang, J.-H. Ahn and H.-G. Hur, *Appl. Biol. Chem.*, 2020, **63**, 27.
9 P. Devi, A. Soni and J. P. Singh, *J. Polym. Res.*, 2024, **31**, 152.
10 S. Kim, D. Kong, X. Zheng and J. H. Park, *J. Energy Chem.*, 2024, **91**, 522–541.
11 L. Mais, N. Melis, A. Vacca and M. Mascia, *Environ. Sci. Water Res. Technol.*, 2024, **10**, 399–407.
12 A. J. Chirinos-Padrón, P. H. Hernández, E. Chávez, N. S. Allen, C. Vasiliou and M. DePoortere, *Eur. Polym. J.*, 1987, **23**, 935–940.
13 J. E. Rorrer, G. T. Beckham and Y. Román-Leshkov, *JACS Au*, 2021, **1**, 8–12.
14 G. Celik, R. M. Kennedy, R. A. Hackler, M. Ferrandon, A. Tennakoon, S. Patnaik, A. M. LaPointe, S. C. Ammal, A. Heyden, F. A. Perras, M. Pruski, S. L. Scott, K. R. Poeppelmeier, A. D. Sadow and M. Delferro, *ACS Cent. Sci.*, 2019, **5**, 1795–1803.
15 C. Sun, J. Wang, J. Wang, M. Shakouri, B. Shi, X. Liu, Y. Guo, Y. Hu, X.-P. Wu and Y. Wang, *Appl. Catal. B Environ. Energy*, 2024, **353**, 124046.
16 Y. Yuan, Z. Xie, K. K. Turaczy, S. Hwang, J. Zhou and J. G. Chen, *Chem Bio Eng.*, 2024, **1**, 67–75.
17 V. D. Knyazev, *J. Phys. Chem. A*, 2007, **111**, 3875–3883.
18 I. Alkorta and J. Elguero, *Chem. Phys. Lett.*, 2006, **425**, 221–224.
19 G. Kresse and J. Furthmüller, *Phys. Rev. B*, 1996, **54**, 11169–11186.
20 G. Kresse and J. Furthmüller, *Comput. Mater. Sci.*, 1996, **6**, 15–50.
21 S. R. Bahn and K. W. Jacobsen, *Comput. Sci. Eng.*, 2002, **4**, 56–66.
22 G. Kresse and D. Joubert, *Phys. Rev. B*, 1999, **59**, 1758–1775.
23 B. Hammer, L. B. Hansen and J. K. Nørskov, *Phys. Rev. B*, 1999, **59**, 7413–7421.
24 S. Grimme, J. Antony, S. Ehrlich and H. Krieg, *J. Chem. Phys.*, 2010, **132**, 154104.
25 Z.-P. Liu and P. Hu, *J. Am. Chem. Soc.*, 2003, **125**, 1958–1967.
26 L. Bengtsson, *Phys. Rev. B*, 1999, **59**, 12301–12304.
27 A. Heyden, A. T. Bell and F. J. Keil, *J. Chem. Phys.*, 2005, **123**, 224101.
28 S. Goedecker, *J. Chem. Phys.*, 2004, **120**, 9911–9917.
29 C. L. Zitnick, L. Chanussot, A. Das, S. Goyal, J. Heras-Domingo, C. Ho, W. Hu, T. Lavril, A. Palizhati, M. Riviere, M. Shuaibi, A. Sriram, K. Tran, B. Wood, J. Yoon, D. Parikh and Z. Ulissi, *arXiv*, 2020, preprint, arXiv:arXiv:2010.09435, DOI: 10.48550/arXiv.2010.09435.
30 Meta AI and Carnegie Mellow University, Open Catalyst Project, https://opencatalystproject.org/.
31 L. Chanussot, A. Das, S. Goyal, T. Lavril, M. Shuaibi, M. Riviere, K. Tran, J. Heras-Domingo, C. Ho, W. Hu, A. Palizhati, A. Sriram, B. Wood, J. Yoon, D. Parikh, C. L. Zitnick and Z. Ulissi, *ACS Catal.*, 2021, **11**, 6059–6072.
32 R. Tran, J. Lan, M. Shuaibi, B. M. Wood, S. Goyal, A. Das, J. Heras-Domingo, A. Kolluru, A. Rizvi, N. Shoghi, A. Sriram, F. Therrien, J. Abed, O. Voznyy, E. H. Sargent, Z. Ulissi and C. L. Zitnick, *ACS Catal.*, 2023, **13**, 3066–3084.
33 J. Musielewicz, X. Wang, T. Tian and Z. Ulissi, *Mach. Learn. Sci. Technol.*, 2022, **3**, 03LT01.
34 B. A. Sexton and A. E. Hughes, *Surf. Sci.*, 1984, **140**, 227–248.
35 S. L. Tait, Z. Dohnálek, C. T. Campbell and B. D. Kay, *J. Chem. Phys.*, 2006, **125**, 234308.
36 X. Ding, H. Zhu, H. Ren, D. Liu, Z. Yu, N. Shi and W. Guo, *Phys. Chem. Chem. Phys.*, 2020, **22**, 21835–21843.
37 S. W. Benson and J. H. Buss, *J. Chem. Phys.*, 1958, **29**, 546–572.
38 M. Salciccioli, Y. Chen and D. G. Vlachos, *J. Phys. Chem. C*, 2010, **114**, 20155–20166.

The data supporting this article have been included as part of the Supplementary Information.